Boosting heterojunction interaction in electrochemical construction of MoS_2 quantum dots@TiO_2 nanotube arrays for highly effective photoelectrochemical performance and electrocatalytic hydrogen evolution

Jianing Dong [a], Xinnan Zhang [a], Jianying Huang [a, b], Shouwei Gao [a], Jiajun Mao [a], Jingsheng Cai [a], Zhong Chen [c], Sanjayan Sathasivam [d], Claire J. Carmalt [d], and Yuekun Lai [a, b, *]

[a] National Engineering Laboratory for Modern Silk, College of Textile and Clothing Engineering, Soochow University, Suzhou 215123, P. R. China.

[b] College of Chemical Engineering, Fuzhou University, Fuzhou 350116, P. R. China.

[c] School of Materials Science and Engineering, Nanyang Technological University, 50 Nanyang Avenue, Singapore.

[d] Department of Chemistry, University College London, London, WC1H 0AJ, United Kingdom

E-mail: yklai@suda.edu.cn

ABSTRACT: MoS_2 quantum dots (QDs) are loaded onto TiO_2 nanotube arrays (NTAs) via a facile strategy of combining electrochemical exfoliation with electrophoretic deposition (EFED). The optimal MoS_2@TiO_2 NTAs exhibits a low onset potential (76 mV vs RHE) with the Tafel slope of 93 mV dec^{-1}. The reported synthesis strategy is suitable for the heterojunction construction of other two-dimensional layered materials and semiconductor composites with excellent photoelectric properties.

Keywords: MoS_2 quantum dots, TiO_2 nanotube arrays, Electrochemical exfoliation, Electrophoretic deposition, Hydrogen evolution reaction

1. Introduction

Since Fujishima and Honda reported photocatalytic water splitting using titanium dioxide (TiO_2) in 1972 [1], TiO_2 has been extensively developed in several application fields, including photocatalytic degradation of organic contaminants [2], hydrogen production by water splitting [3] and dye-sensitized solar cells [4]. Among various nanostructure forms, TiO_2 nanotube arrays (NTAs) have garnered considerable attention due to its large specific surface area and efficiently oriented charge transfer route [5]. Therefore, TiO_2 NTAs can provide a large surface area for efficient electrocatalyst loading and boost the electrocatalytic activity. Moreover, TiO_2 NTAs offer a large amount of active sites and if an efficient heterojunction can be formed with other semiconductors, the nanocomposites could have a high potential for photoelectric properties. Therefore, a facile strategy is urgently required to design an efficient heterojunction with TiO_2 NTAs on the photoelectric properties and electrocatalytic for hydrogen evolution.

In recent years, molybdenum sulfide (MoS_2), as a kind of the layered transition metal dichalcogenide, has been widely investigated [6,7]. Recent studies verify that MoS_2 is an excellent electrocatalyst for the hydrogen evolution reaction owing to its edge defects [8]. To be highly effective, ultra-thin MoS_2 nanosheets are necessary to fully expose their edge defects and achieve maximum quantum confinement effects. Thus, constructing MoS_2 nanodots are a promising strategy to enhance the efficiency of hydrogen evolution reaction (HER). Previous reports of MoS_2 QDs include sonication and hydrothermal treatment [9], liquid exfoliation [10] and ball milling

with chemical Li-intercalation [11], however, these synthetic approaches are sensitive to the conditions and are limited by time consumption, harsh environments and toxic organic solvents. Usually, MoS_2 nanodots are supported on Au foil, Pt piece and other conductive substrates to carry out the hydrogen evolution reaction [12]. Nevertheless, the huge cost and complex preparation hinder practical applications for the future. In these contexts, it is necessary to develop a facile technique to obtain MoS_2 quantum dots loaded on promising substrates such as TiO_2, carbon materials, and so on.

Herein, we propose a convenient electrochemical exfoliation and electrophoretic deposition (EFED) strategy to rationally design MoS_2@TiO_2 NTAs heterojunction. With the synergistic advantages, the boosting of the interfacial heterojunction interaction between the TiO_2 NTAs and the decorated MoS_2 quantum dots displays a substantial increase in photoelectric property and electrocatalytic hydrogen evolution.

2. Materials and methods

Vertical-aligned TiO_2 NTAs were prepared by a convenient two-step anodization strategy [13]. The highly crystalline MoS_2 quantum dots were prepared via an electrochemical exfoliation method [14]. In the current work, 0.5 g MoS_2 powder (purchased from Aladdin, 99.5%) was compressed into a bulk by applying a continuous pressure of 15.0 MPa for 60 s. Then, 20 ml DI water containing 0.1 wt% lithium bis(trifluoromethane) sulfonamide (LiTFSI) salt (purchased from Aladdin) was employed as electrolyte. The bulk MoS_2 was used as the anode and the prepared TiO_2 NTAs was as the cathode under 5.0 V voltage. The distance between the electrodes was kept at 1.0 cm. The MoS_2@TiO_2 NTA-0.5, 1.0 and 2.0 refers to

different EFED time for 0.5, 1.0 and 2.0 hours. The synthesis route is shown in Scheme 1.

Scheme 1. The illustration of the preparation of the hierarchical MoS_2@TiO_2 NTAs.

The morphologies of MoS_2@TiO_2 NTAs were characterized using a transmission electron microscope (TEM, FEI Tecnai G-20). The structural characterization of the MoS_2@TiO_2 NTAs was carried out using a high-resolution transmission electron microscope (HRTEM). The crystal phase was determined by an X-ray diffractometer with Cu-Kα radiation (XRD, Philips, X'pert-Pro MRD). To confirm the surface chemical compositions, X-ray photoelectron spectroscopy (XPS, KRATOS, Axis Ultra HAS) was employed. Photoluminescence (PL) measurement was made using a fluorescence spectroscope (HORIBA JOBIN YVON, FM4P-TCSPC).

An electrochemical workstation (AUTOLAB, Switzerland) was used to carry out the photocurrent measurement and electrochemical impedance spectroscopic (EIS) measurement in a three-electrode system: TiO_2 NTAs/MoS_2@TiO_2 NTAs was used as the working electrode, Pt foil as the counter electrode, and the saturated Ag/AgCl electrode as the reference electrode. The test conditions are as follows [15]: The 0.1 M Na_2SO_4 aqueous solution was utilized as electrolyte (pH=6.8). A GY-10 xenon lamp with a power density around 100 mW cm^{-2}, was used to offer the light illumination. The EIS measurements were carried out at a frequency range of 10^5-10^{-1} Hz. The J-V curves were obtained by a scan rate of 10.0 mV s^{-1}.

The electrocatalytic activity for hydrogen evolution of MoS_2@TiO_2 NTAs was

tested by the same three-electrode system in a 0.5 M H_2SO_4 electrolyte. The properties of hydrogen evolution were measured by linear sweep voltammetry at 2.0 mV s^{-1}. To avoid the Pt deposition during the CV testing, a graphite rod instead of Pt was used. The stability was studied by cyclic voltammetry for 1000 cycles at a rate of 0.1 V s^{-1}.

3. Results and discussion

The single TiO_2 NTAs decorated by uniformed MoS_2 QDs is displayed in Figure 1a. MoS_2 quantum dots were anchored on the inner and outer tubes of TiO_2 NTAs with the size of 2.0~3.0 nm and the average diameter was 2.7 nm The HRTEM and SAED is depicted in Figure 1b-d and the high-resolution TEM elemental area mapping of a single tube is shown in Figure 1e-1h.

Figure 1. (a) MoS_2@TiO_2 NTAs TEM images. (b, c) HRTEM images of the selected area (in red circles of a) and (d) SAED pattern for the images of (b). (e-h) Elemental mapping in single MoS_2@TiO_2 NTAs, the scale bars are 20 nm for all.

The XRD spectra of the three specimens: MoS_2, TiO_2 NTAs and the MoS_2@TiO_2 nanostructure composites are shown in Figure 2a. The diffraction maximum at 25.3°, 37.9°, 48.0° and 53.9° can be assigned to the (101), (004), (200) and (105) facets of the TiO_2 anatase phase. Peaks belonging to the (002), (100), (103), (105), (110), (008) planes of MoS_2 were detected in the bulk sample, however, after exfoliation into quantum dots, only a weak peak at 32.0° was present in the MoS_2@TiO_2 sample, implying that the MoS_2 QDs contain only few layers. Figure 2b shows the Raman

spectrum of the TiO_2 NTAs, MoS_2 bulk and MoS_2@TiO_2 NTAs nanocomposites. The characteristic Raman band with E_{1g} = 145 cm^{-1}, B_{1g} = 392 cm^{-1}, A_{1g} = 513 cm^{-1}, E_g = 634 cm^{-1} confirm the presence of anatase TiO_2. Furthermore, Raman peaks corresponding to MoS_2@TiO_2 nanocomposites were observed at 380 cm^{-1}, 401 cm^{-1} and 452 cm^{-1} and attributed to the E_{2g}^1, A_{1g} and E_{1U}^2 modes, respectively. Figure 2c-2d shows the XPS spectra and PL intensity of pure TiO_2 NTAs and the MoS_2@TiO_2 composites. The summary XPS spectra peak at Ti 2p (458.9 eV), O 1s (532.4 eV), and C 1s (284.5 eV) can be observed in both pure TiO_2 NTAs and MoS_2@TiO_2 NTAs. Moreover, compared with the MoS_2 bulk, the slight peak intensity of Mo 3p, Mo 3d and S 2p can be observed in MoS_2@TiO_2 NTAs due to the high dispersion and the small size of MoS_2 QDs. Compared to the pure TiO_2 NTAs, the MoS_2@TiO_2 composites display a lower PL intensity from 400 to 650 nm, which signifies a faster electronic transmission and a higher electrocatalytic activity at the interfacial heterojunction interaction. In the high-solution XPS spectra (Figure 2e, f), binding energy peaks for Mo $3d_{5/2}$ and Mo $3d_{3/2}$ at 232.2 eV and 229.2 eV correspond to the presence of Mo^{4+}. The peaks at 162.2 eV and 163.5 eV are fitted to S $2p_{3/2}$ and S $2p_{1/2}$.

Figure 2. (a) The XRD and (b) Raman spectra of MoS_2 bulk, TiO_2 NTAs, MoS_2@TiO_2 NTAs. (c) XPS spectra and (d) PL spectra of pristine TiO_2 NTAs and MoS_2@TiO_2 NTAs. The high resolution XPS spectra of (e) Mo 3d, (f) S 2p of MoS_2@TiO_2 NTAs.

Figure 3a shows the current-time (I-t) responses of pure TiO_2 NTAs and MoS_2@TiO_2 NTA-0.5, 1.0 and 2.0 h electrodes with a turn-in frequency of 30 s. The electrochemical performance was measured by electrochemical impedance spectroscopy. As shown in Figure 3b, under both dark and simulated solar light irradiation, the plain TiO_2 NTAs had a larger diameter of semi-circular curves, indicating a poor interaction conductivity at the heterojunction interface. However, the TiO_2 NTAs supported by MoS_2 quantum dots showed a smaller diameter owing to the reduced electron-hole recombination at the interfacial interaction of the heterojunction structure of MoS_2 QDs on TiO_2 NTAs. The enhanced photoelectric performance was confirmed by the J-V curves (Figure 3c). At the 0.8 V bias, the photocurrent density reached 0.83 mA cm^{-2}, which is 2.6 times that of the pure TiO_2 sample. In Figure 3d, the hierarchical MoS_2@TiO_2 NTAs-1 electrode shows an optimal η at 0.46% under an applied bias of 0.5 V.

Figure 3. (a) Photocurrent responses for pristine TiO_2 NTAs and MoS_2@TiO_2 NTAs; (b) EIS plots for pristine TiO_2 NTAs and MoS_2@TiO_2 NTAs; (c) J-V curves of 10 mV s^{-1} for TiO_2 NTAs and MoS_2@TiO_2 NTAs-1 electrodes; (d) Photoconversion efficiency with different electrodes (TiO_2 NTAs and MoS_2@TiO_2 NTAs-1).

The linear sweep voltammetry (LSV) of hydrogen evolution reactions can be measured by LSV curve (Figure 4a). Due to the active edge of MoS_2 QDs, exfoliated MoS_2 nanodots loaded on the TiO_2 NTAs show a significant electrocatalytic activity with a low onset potential about 76 mV at 1.0 mA cm^{-2}. The low onset potential can be ascribed to the specific micro/nanopores structure of the MoS_2@TiO_2 NTAs-1,

which favors mass transfer and reduces the concentration polarization. The overpotential of MoS_2@TiO_2 NTAs-1 was 162 mV at the current density of 10 mA cm^{-2} due to the high Tafel slope that will be discussed later.

The Tafel plots were measured to further investigate the HER activity (Figure 4b), the slope of MoS_2@TiO_2 NTAs-1 was found to be 93 mV dec^{-1}, higher than the 33 mV dec^{-1} of best known catalyst, Pt, due to the lower conductivity of MoS_2. After 1000 cycles, slight inactivation was observed, suggesting a good stability of the MoS_2@TiO_2 NTAs (Figure 4c). Figure 4d compares with the overpotential at 10 mA cm^{-2} current density and the corresponding Tafel slope of various MoS_2-based and TiO_2-based electrocatalysts [16-27].

Figure 4. (a) The linear sweep voltammetry of TiO_2 NTAs, MoS_2@TiO_2 NTAs-1, Pt sheet; (b) The corresponding Tafel curves for the MoS_2@TiO_2 NTAs-1 and Pt sheet; (c) Stability test of the MoS_2@TiO_2 NTAs-1 scan in 0.5 M H_2SO_4 at a scan rate of 100 mV s^{-1}. (d) Comparison of the overpotentials at a current density of 10 mA cm^{-2} and the Tafel slope for different MoS_2-based and TiO_2-based catalysts.

4. Conclusions

In summary, we have developed a strategy to construct the hierarchical MoS_2@TiO_2 NTAs by using a method combining electrochemical exfoliation with electrophoretic deposition. The MoS_2@TiO_2 NTAs not only display a highly photoelectric ability, but also possess an outstanding property of electrocatalytic for hydrogen evolution with a low onset potential of 76 mV dec^{-1}. This outstanding performance of MoS_2@TiO_2 NTAs can be attributed to the boosting interfacial

heterojunction interaction in the photo-excited electron transfer and the high electrocatalytic activity of the quantum dots.

Acknowledgements

The authors acknowledge the National Natural Science Foundation of China (21501127 and 51502185).

References

[1] A. Fujishima, K. Honda, Electrochemical photolysis of water at a semiconductor electrode, Nature 238 (1972) 37-38.

[2] Y.B. Liu, Q.F. Yao, X.J. Wu, T.K. Chen, Y. Ma, C.N. Onga, J.P. Xie, Gold nanocluster sensitized TiO_2 nanotube arrays for visible-light driven photoelectrocatalytic removal of antibiotic tetracycline, Nanoscale 8 (2016) 10145-10151.

[3] M.D. Ye, J.J. Gong, Y.K. Lai, C.J. Lin, Z.Q. Lin, High-efficiency photoelectrocatalytic hydrogen generation enabled by palladium quantum dots-sensitized TiO_2 nanotube arrays, J. Am. Chem. Soc. 134 (2012) 15720-15723.

[4] G.K. Mor, K. Shankar, M. Paulose, O.K. Varghese, C.A. Grimes, Use of highly-ordered TiO_2 nanotube arrays in dye-sensitized solar cells, Nano Lett. 6 (2006) 215-218.

[5] Y.B. Liu, J.H. Li, Ba.X. Zhou, H.C. Chen, Z.S. Wang, W.M. Cai, A TiO_2-nanotube-array-based photocatalytic fuel cell using refractory organic

compounds as substrates for electricity generation, Chem. Commun. 47 (2011) 10314-10316.

[6] X.M. Zhou, M. Licklederer, P. Schmuki, Thin MoS_2 on TiO_2 nanotube layers: An efficient co-catalyst/harvesting system for photocatalytic H_2 evolution, Electrochem. Commun. 73 (2016) 33-37.

[7] Q. Ding, B. Song, P. Xu, S. Jin, Efficient electrocatalytic and photoelectrochemical hydrogen generation using MoS_2 and related compounds, Chem, 1 (2016) 699-726.

[8] J.F. Xie, H. Zhang, S. Li, R.X. Wang, X. Sun, M. Zhou, J.F. Zhou, X.W. Lou, Y. Xie, Defect-rich MoS_2 ultrathin nanosheets with additional active edge sites for enhanced electrocatalytic hydrogen evolution, Adv. Mater. 25 (2013) 5807-5813.

[9] S.C. Chen, C.Y. Lin, T.L. Cheng, W.L. Tseng, 6- mercaptopurine- induced fluorescence quenching of monolayer MoS_2 nanodots: applications to glutathione sensing, cellular imaging, and glutathione- stimulated drug delivery, Adv. Funct. Mater. 27 (2017) 1702452.

[10] D. Gopalakrishnan, D. Damien, M.M. Shaijumon, MoS_2 quantum dot-interspersed exfoliated MoS_2 nanosheets, ACS Nano 8 (2014) 5297-5303.

[11] C.L. Tan, Z.M. Luo, A. Chaturvedi, Y.Q. Cai, Y.H. Du, Y. Gong, Y. Huang, Z.C. Lai, X. Zhang, L.R. Zheng, X.Y. Qi, M.H. Goh, J. Wang, S.K. Han, X.J. Wu, L. Gu, C. Kloc, H. Zhang, Preparation of high-percentage 1T-phase transition metal dichalcogenide nanodots for electrochemical hydrogen evolution, Adv. Mater. 30 (2018) 1705509.

[12] D. Damien, A. Anil, D. Chatterjee, M.M. Shaijumon, Direct deposition of $MoSe_2$ nanocrystals onto conducting substrates: towards ultra-efficient electrocatalysts for hydrogen evolution, J. Mater. Chem. A, 5 (2017) 13364-13372.

[13] J.S. Cai, J.Y. Huang, Y.K. Lai, 3D Au-decorated Bi_2MoO_6 nanosheet/TiO_2 nanotube array heterostructure with enhanced UV and visible-light photocatalytic activity, J. Mater. Chem. A, 5 (2017) 16412-16421.

[14] D. Gopalakrishnan, D. Damien, B. Li, H. Gullappalli, V.K. Pillai, P.M. Ajayan, M.M. Shaijumon, Electrochemical synthesis of luminescent MoS_2 quantum dots, Chem. Commun. 51 (2015) 6293-6296.

[15] Q.P. Chen, J.H. Li, B.X. Zhou, M.C. Long, H.C. Chen, Y.B. Liu, W.M. Cai, W.F. Shangguan, Preparation of well-aligned WO_3 nanoflake arrays vertically grown on tungsten substrate as photoanode for photoelectrochemical water splitting, Electrochem. Commun. 20 (2012) 153-156.

[16] Y.C. Chen, A.Y. Lu, P. Lu, X.L. Yang, C.M. Jiang, M. Mariano, B. Kaehr, O. Lin, A. Taylor, I.D. Sharp, L.J. Li, S.S. Chou, V. Tung, Structurally deformed MoS_2 for electrochemically stable, thermally resistant, and highly efficient hydrogen evolution reaction, Adv. Mater. 29 (2017) 1703863.

[17] D.R. Cummins, U. Martinez, A. Sherehiy, R. Kappera, A.M. Garcia, R.K. Schulze, J. Jasinski, J. Zhang, R.K. Gupta, J. Lou, M. Chhowalla, G. Sumanasekera, A.D. Mohite, M.K. Sunkara, G. Gupta, Efficient hydrogen evolution in transition metal dichalcogenides via a simple one-step hydrazine reaction, Nat. Commun. 7 (2016) 11857.

[18] S.J. Xu, D. Li, P.Y. Wu, One-pot, facile, and versatile synthesis of monolayer MoS_2/WS_2 quantum dots as bioimaging probes and efficient electrocatalysts for hydrogen evolution reaction, Adv. Funct. Mater. 25 (2015) 1127-1136.

[19] H.D. Yu, Y.R. Xue, L. Hui, C. Zhang, Y.J. Zhao, Z.B. Li, Y.L. Li, Controlled growth of MoS_2 nanosheets on 2D N-doped graphdiyne nanolayers for highly associated effects on water reduction, Adv. Funct. Mater. 28 (2018) 1707564.

[20] S.J. Kim, D.W. Kim, J. Lim, S.Y. Cho, S.O. Kim, H.T. Jung, Large-area buckled MoS_2 films on the graphene substrate, ACS Appl. Mater. Interfaces 8 (2016) 13512-13519.

[21] Z.H. Zhao, F. Qin, S. Kasiraju, L.X. Xie, M.K. Alam, S. Chen, D.Z. Wang, Z.F. Ren, Z.M. Wang, L.C. Grabow, J.M. Bao, Vertically aligned MoS_2/Mo_2C hybrid nanosheets grown on carbon paper for efficient electrocatalytic hydrogen evolution, ACS Catal. 7 (2017) 7312-7318.

[22] H. Li, C. Tsai, A.L. Koh, L.L. Cai, A.W. Contryman, A.H. Fragapane, J.H. Zhao, H.S. Han, H.C. Manoharan, F.A. Pedersen, J.K. Nørskov, X.L. Zheng, Activating and optimizing MoS_2 basal planes for hydrogen evolution through the formation of strained sulphur vacancies, Nat. Mater. 15 (2015) 48-53.

[23] J. Kibsgaard, Z.B. Chen, B.N. Reinecke, T.F. Jaramillo, Engineering the surface structure of MoS_2 to preferentially expose active edge sites for electrocatalysis, Nat. Mater. 11 (2012) 963-969.

[24] Y. Shi, J. Wang, C. Wang, T.T. Zhai, W.J. Bao, J.J. Xu, X.H. Xia, H.Y. Chen, Hot electron of Au nanorods activates the electrocatalysis of hydrogen evolution on MoS_2 nanosheets, J. Am. Chem. Soc. 137 (2015) 7365-7370.

[25] B. Jin, X.M. Zhou, L. Huang, M. Licklederer, M. Yang, P. Schmuki, Aligned MoOx/MoS_2 core-shell nanotubular structures with a high density of reactive sites based on self-ordered anodic molybdenum oxide manotubes, Angew. Chem. Int. Ed. 55 (2016) 12252-12256.

[26] X. Cheng, Y.H. Li, L.R. Zheng, Y. Yan, Y.F. Zhang, G. Chen, S.R. Sun, J.J. Zhang, Highly active, stable oxidized platinum clusters as electrocatalysts for the hydrogen evolution reaction, Energy Environ. Sci. 10 (2017) 2450-2458.

[27] J.Y. Yu, W.J. Zhou, T.L. Xiong, A.L. Wang, S.W. Chen, B.L. Chu, Enhanced electrocatalytic activity of Co@N-doped carbon nanotubes by ultrasmall defect-rich TiO_2 nanoparticles for hydrogen evolution reaction, Nano Res. 10 (2017) 2599-2609.

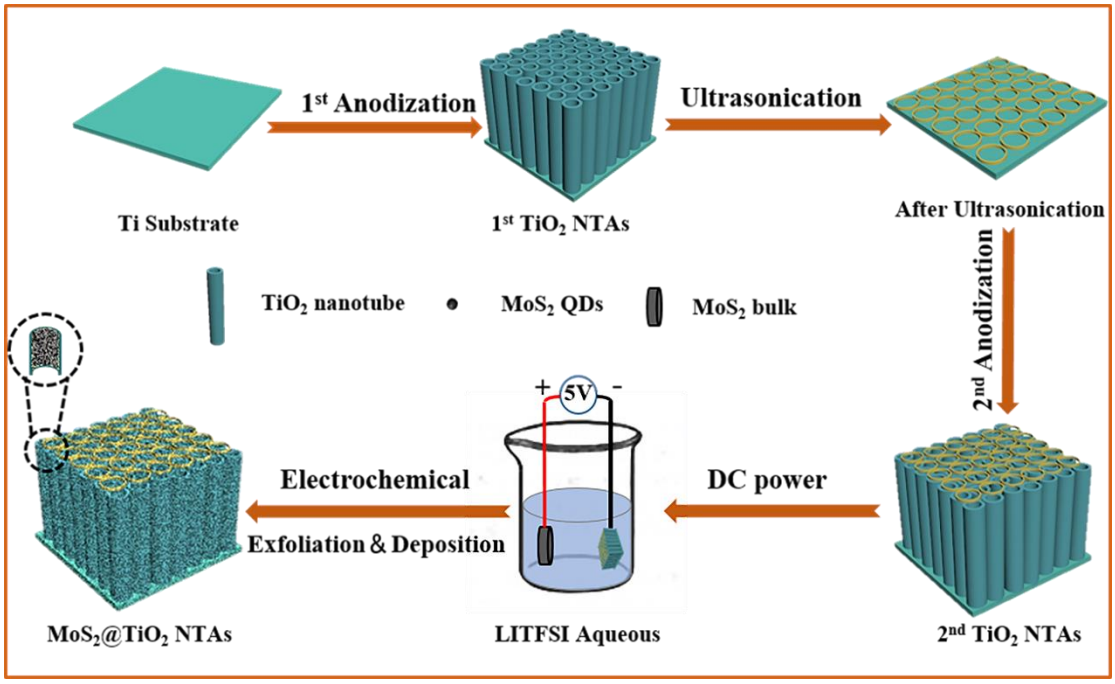

Scheme 1

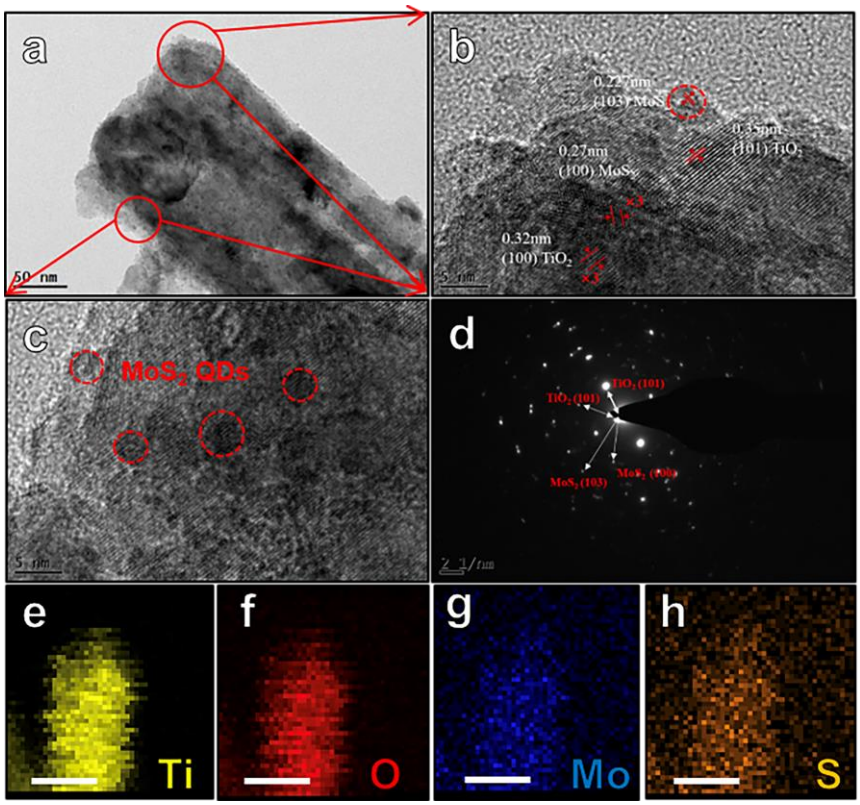

Figure 1

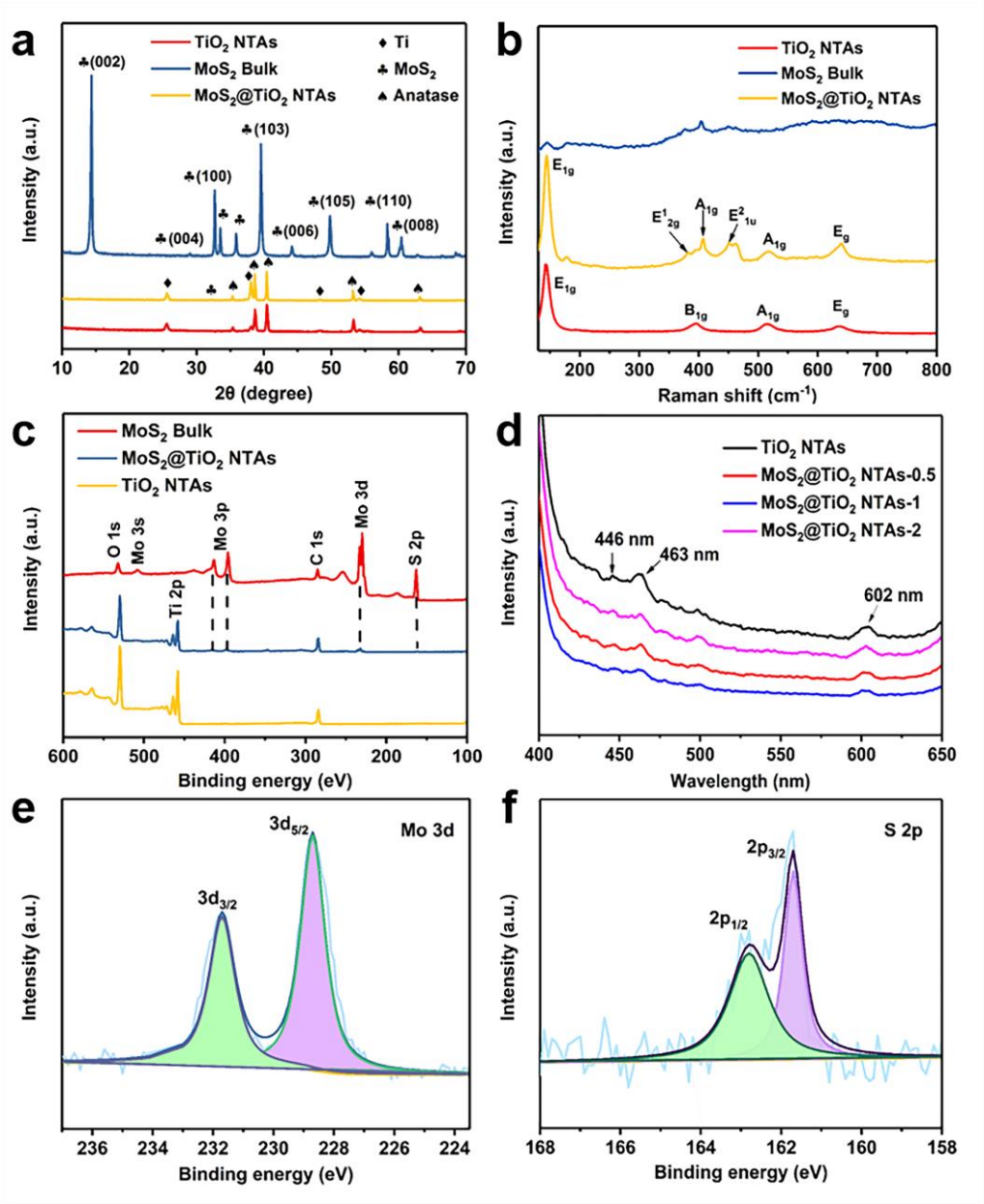
a
TiO2 NTAs
MoS2 Bulk
MoS2@TiO2 NTAs
Ti
MoS2
Anatase
♣(002)
♣(103)
♣(100)
♣(004)
♣(006)
♣(105)
♣(110)
♣(008)
Intensity (a.u.)
2θ (degree)
b
TiO2 NTAs
MoS2 Bulk
MoS2@TiO2 NTAs
E1g
E12g
A1g
E21u
A1g
Eg
B1g
Raman shift (cm-1)
c
MoS2 Bulk
MoS2@TiO2 NTAs
TiO2 NTAs
O 1s
Mo 3s
Ti 2p
Mo 3p
C 1s
Mo 3d
S 2p
Binding energy (eV)
d
TiO2 NTAs
MoS2@TiO2 NTAs-0.5
MoS2@TiO2 NTAs-1
MoS2@TiO2 NTAs-2
446 nm
463 nm
602 nm
Wavelength (nm)
e
Mo 3d
3d5/2
3d3/2
Binding energy (eV)
f
S 2p
2p3/2
2p1/2
Binding energy (eV)

Figure 2

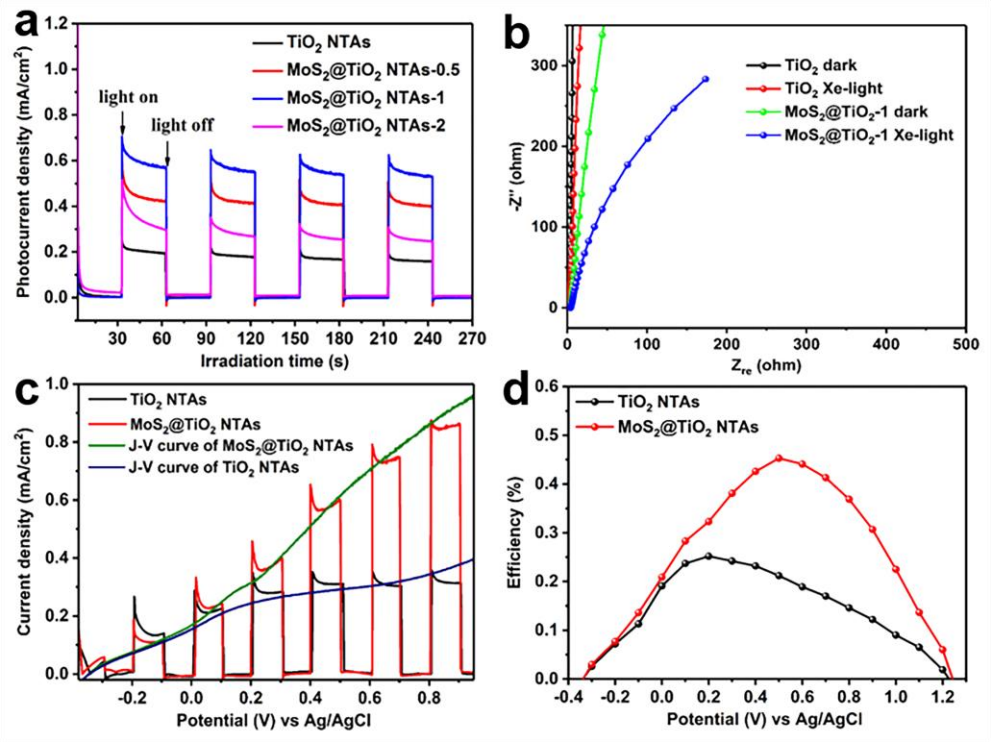

Figure 3

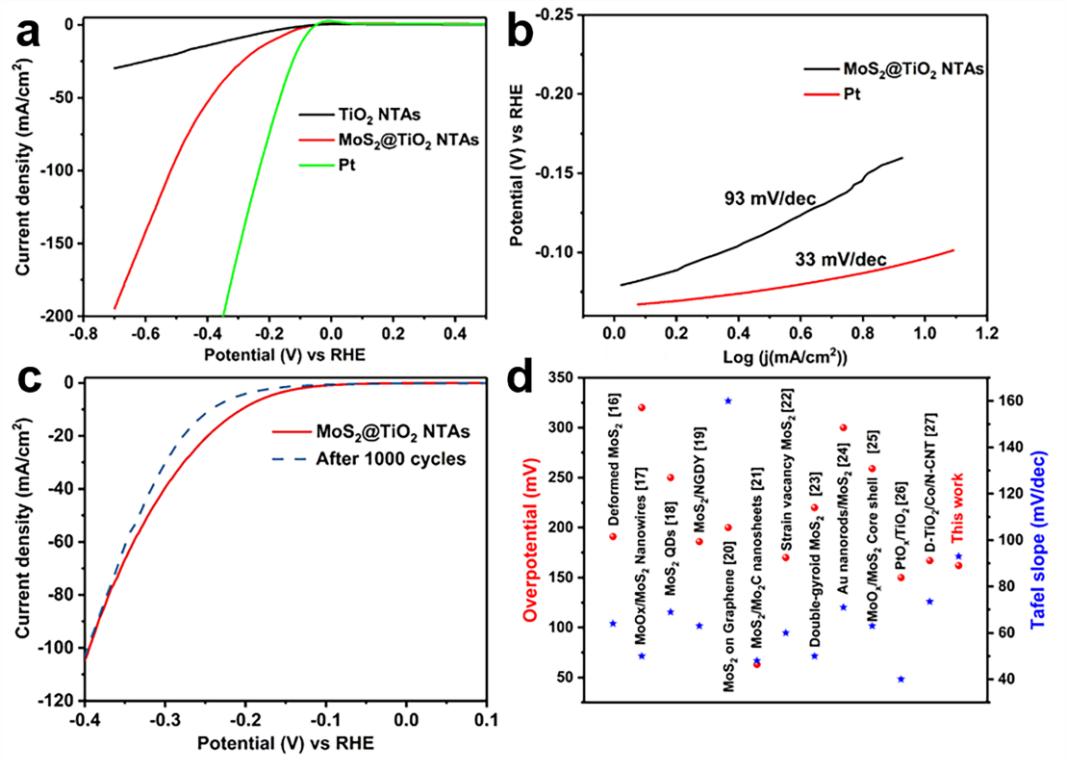

Figure 4